EFDA–JET–PR(06)19

J. Ongena, A. Ekedahl, L.-G. Eriksson, J.P. Graves, M.-L. Mayoral, J. Mailloux, V. Petrzilka, S.D. Pinches, K. Rantamaki, Yu. Baranov, L. Bertalot, C.D. Challis, G. Corrigan, K. Erents, M. Goniche, T. Hellsten, I. Jenkins, T. Johnson, D.L. Keeling, V. Kiptily, P.U. Lamalle, M. Laxåback, E. Lerche, M.J. Mantsinen, J.-M. Noterdaeme, V. Parail, S. Popovichev, A. Salmi, M. Santala, J. Spence, S. Sharapov, A.A. Tuccillo, D.Van Eester and JET EFDA contributors

Recent Progress in JET on Heating and Current Drive Studies in View of ITER

Recent Progress in JET on Heating and Current Drive Studies in View of ITER

J. Ongena[1], A. Ekedahl[2], L.-G. Eriksson[2], J.P. Graves[3], M.-L. Mayoral[4], J. Mailloux[4], V. Petrzilka[5], S.D. Pinches[4], K. Rantamaki[11], Yu. Baranov[4], L.Bertalot[6], C.D. Challis[4], G. Corrigan[4], K. Erents[4], M. Goniche[3], T. Hellsten[7], I. Jenkins[4], T. Johnson[7], D.L. Keeling[4], V. Kiptily[4], P.U. Lamalle[1], M. Laxåback[7], E. Lerche[1], M.J. Mantsinen[9], J.-M. Noterdaeme[8,10], V. Parail[4], S. Popovichev[4], A. Salmi[9], M. Santala[8], J. Spence[4], S. Sharapov[4], A.A. Tuccillo[6], D.Van-Eester[1] and JET EFDA contributors*

[1]Plasma Physics Laboratory, Royal Military Academy, Association EURATOM - Belgian State, Brussels, Belgium[+]
[2]Association EURATOM-CEA, CEA/DSM/DRFC, CEA Cadarache, F-13108 St Paul lez Durance, France
[3]Centre de Recherches en Physique des Plasmas (CRPP), École Polytechnique Fédérale de Lausanne, Association EURATOM – Confédération Suisse, 1015 Lausanne, Switzerland
[4] EURATOM/UKAEA Fusion Association, Culham Science Centre, Abingdon, UK
[5] Association EURATOM-IPP.CR, Za Slovankou 3, 182 21 Praha 8, Czech Republic
[6] Associazione EURATOM-ENEA sulla Fusione, Frascati, Italy
[7] Alfvén Laboratory, KTH, EURATOM-VR Association, Sweden
[8] Max-Planck IPP-EURATOM Association, Garching, Germany
[9] HUT, Association EURATOM-Tekes, Helsinki, Finland
[10] Gent University, EESA, Belgium
[11] Association EURATOM-Tekes, VTT, P.O.Box 1000, Espoo, FI-02044 VTT, Finland
[b]Partner in the Trilateral Euregio Cluster (TEC)
** See annex of M.L. Watkins et al, "Overview of JET Results ", (Proc. 21st IAEA Fusion Energy Conference, Chengdu, China (2006)).*

Preprint of Paper to be submitted for publication in
Nuclear Fusion

ABSTRACT.
Experiments have been performed investigating the use of Ion Cyclotron Current Drive (ICCD) for sawtooth destabilization. The analysis allows for a generalization to any method capable of driving current close to the q=1 surface. A detailed study of the inverted ICRF heating scenarios, to be used in the hydrogen phase of ITER, shows the sensitivity of such scenarios to small concentrations of impurities having the same charge to mass ratio as the D minority ions. Their presence prevents any D minority heating, as the fast wave cannot longer reach the D ion cyclotron resonance layer. This has possible implications for the choice of the ICRF heating scenario in the hydrogen phase of ITER. An improved understanding has been obtained for the evolution of the density in the Scrape Off Layer (SOL) with strong gas puffing (to improve coupling) during high power Low Hybrid (LH) operation. Agreement with experiment can only be obtained assuming that LH power losses in the SOL increase ionization.

INTRODUCTION.
For a successful operation of ITERs baseline scenarios, heating and current drive systems will be essential to initiate, sustain and control the largely-self-heated fusion burn, to optimize the current profile and contribute to eliminate instabilities. Continued progress in optimizing these systems and in the understanding of the physics involved is important to accelerate the ITER operational phase and this paper summarizes recent results obtained on JET in this field of research.

1. CONTROL OF SAWTEETH USING ICCD
Fast alpha particles in a tokamak reactor have the potential to induce sawteeth with long periods. While long sawtooth free periods in themselves do not have any detrimental effect on the plasma performance, the crashes associated with them can trigger unwanted Magneto HydroDynamic (MHD) activity. In particular, crashes after long sawtooth free periods could generate seed islands for Neo-classical Tearing Modes (NTMs) as reported in earlier experiments [1, 2]. Since the presence of NTMs can degrade the plasma performance it is important to either control or avoid triggering of them. One possibility to avoid NTMs is to avoid large sawtooth crashes i.e. keeping the sawtooth period short.

It has previously been shown that the sawtooth period can be controlled by localised Ion Cyclotron Current Drive (ICCD) changing the magnetic shear near the q = 1 surface in JET [3-6]. Theory predicts that an increased shear should have a destabilising effect on the sawteeth whereas a decreased shear should have the opposite effect [7]. However, the experiments reported in Refs. [3-6] were run without any significant presence of fast ions in the centre of the plasma. Since it was not evident that fast ion induced long sawteeth could be as easily affected by ICCD as sawteeth without a significant fast ion population, dedicated experiments with fast ions were carried out on JET in 2003 [8]. These experiments were performed in plasmas with a toroidal magnetic field B_t = 2.7T and plasma current I_p = 2.6MA. The scenario used for both tasks was hydrogen minority in a

deuterium plasma (n_H/n_D ~ 5%) and the available ICRF power in JET was split between two frequencies as follows: (i) a fast hydrogen population was created to generate sawteeth with long induced periods with 42 MHz ICRF heating (corresponding to a central cyclotron resonance (R ~ 3m)); (ii) sawtooth destabilisation using off-axis ICCD near the q = 1 surface on the high field side with 47MHz ICRH heating (corresponding to a H cyclotron resonance layer near the q = 1 surface). Sawtooth destabilisation by ICCD was indeed achieved by phasing the ICRF antennas to launch counter current propagating waves. A short period after the application of the ICCD an effective shortening of the sawtooth period was observed, indicating that the fast ion induced long sawteeth could successfully be destabilised by applying ICCD [8].

Further analysis of the experiments has recently been carried out [9]. The main focus of this analysis has been to simulate the driven currents and the pressure of the fast ions in order to assess in more detail their possible impact on the sawtooth period. To this end, rather comprehensive simulations of the ICRF power deposition and the distribution functions of the resonating ions have been carried out with the SELFO code [10, 11]. This code combines a full wave code with a 3D Monte Carlo solver for the orbit averaged Fokker-Planck equation, and calculates a self-consistent solution. The current profile driven by the ICCD for a discharge with effective shortening of fast ion induced long sawteeth is shown in Fig. 1 and compared to one in a control discharge where the phasing of the antennas was changed to launch waves in the opposite direction (co-current). In the latter no shortening of the sawteeth took place. Recent calculations confirm that for the case with -90 degree phasing the shear at q=1 is larger than the critical shear s_{crit} (s_{crit} ~ 0.2 for this discharge, see Fig. 1), which is one of two simultaneous requirements for instability of the internal kink mode in the ion kinetic regime (see e.g. ref. [7]). The other requirement for instability, which involves the macroscopic stability of the mode, and the response of the fast ions is more complicated, as discussed in [12]. Nevertheless, the enhanced shear at q=1 for the case with –90 degree phasing, especially when compared with the contrasting case with +90 degree phasing is consistent with the short sawteeth observed, and the faster current penetration associated with a faster sawtooth cycle.

2. INVERTED ICRF SCENARIOS

The initial operational phase of ITER will mainly use hydrogen plasmas to minimise the activation of the machine during commissioning. The two relevant ICRF heating schemes foreseen in H plasmas are based on the heating of ^{3}He minority ions or D minority ions. Such scenarios are called inverted scenarios because the ratio of the charge to the mass (Z/A) of the majority ions is larger than that of the minority ions. The main consequence is that the resonance for the fast magnetosonic wave (FW) (referred as the ion-ion hybrid resonance R_{ii}) and the corresponding left cut-off $R_{L\ cut\text{-}off}$ (associated with the left-handed wave polarisation) where the FW can be converted to waves with shorter wavelengths, is between the ICRF antennae and the minority cyclotron resonance layer R_{ic}. The relative position of these layers is inversed compared to standard heating scenarios for which R_{ic} is encountered first by the FW launched by the antenna. Inverted scenarios with ^{3}He minority

ions and D minority heating have recently been tested at JET [13]. A very important conclusion from these experiments analysis is the key role played by a low fraction (n_{imp}/n_e ~1-2%) of C impurity ions (and contributions from all other impurities with Z/A= 1/2) on the effectiveness of these heating scenarios.

This was evident from the following observations. First, with D minority heating in H plasmas ($B_t = 3.9$T, $I_p = 2$MA, 29MHz ICRH, central electron density 3×10^{19} m^{-3}, $n_D/n_e = 1$-2%), no fast D ions were observed, (verified by neutral particle analysis or γ-ray spectrometry). Second, no neutrons were detected and the maximum electron temperature obtained was only around 3 keV. Break-in-Slope (BIS) and Fast Fourier Transform (FFT) analysis [14, 15] performed on the electron temperature response to ICRF power modulation revealed a rather peaked electron power deposition profile maximum (Fig.2) at a major radius R ~ 3.5m (plasma major radius R ~ 3m and plasma minor radius a ~ 1m) with the power absorbed by the electrons estimated to be 50% of total the ICRF power. These results allow us to conclude that instead of having, as expected, a central indirect electron heating by ICRF-accelerated D ions (the ion cyclotron resonance layer radius was at $R_{ic}(D) \approx 3.1$m), off-axis direct electron heating had occurred. This can only be explained by the presence of a low concentration of C ions ($n_C/n_e = 2$-3%) leading predominantly to mode conversion heating.

The effect on the dispersion relation of a C concentration $n_C/n_e = 2\%$ is shown on Fig.3. In Fig 3a, a D concentration of $n_D/n_e = 2\%$ has been assumed and one can see that the FW propagates until it reaches the plasma centre where it undergoes either mode conversion at R_{ii} (and subsequent direct absorption by the electrons) or absorption on the D ions at $R_{ic}(D)$ if the minority ions have a temperature sufficiently high to Doppler broaden $R_{ic}(D)$ beyond $R_{L\ cut\text{-}off}$. Fig. 3b shows the influence on the propagation of the FW by further adding C ions to the plasma at a concentration $n_C/n_e = 2\%$. The effect of the C ions is the same as what would result from the addition of D at a concentration $n_D/n_e = 12\%$, as the C ions act like D ions but with a six times higher concentration. The ion-ion hybrid resonance/left cut-off pair is moved to the tokamak low field side at R ~ 3.5m and the mode conversion regime is expected to dominate. Numerical simulations performed with the 1D code TOMCAT [16] indicate that concentrations as low as 0.5% are sufficient to prevent an efficient absorption at the D minority cyclotron resonance layer. Furthermore, as exemplified by the low and very unsteady antenna coupling during the experiments, the FW wave absorption can indeed be rather poor, resulting in a global pattern of standing waves in the tokamak that strongly influences the power deposition [17]. In order to understand the details of the power absorbed in short wavelengths, modelling has to be performed taking into account realistic profiles, parasitic edge damping and 2-D wave propagation effects. This rather complex problem, requiring massive parallel computer processing capabilities, will be addressed in the near future [18].

It is interesting to note that the effect of the presence of low concentrations of C ions in the plasma on the heating scheme was also observed in ^{3}He minority heating in H plasmas. Successful ^{3}He minority heating was achieved for a concentration of ^{3}He $n_{3He}/n_e < 2\%$, with central electron temperatures up to 6.2keV and energies of the ^{3}He ions in the MeV range using 5MW of ICRF

power. As soon as the ^{3}He concentration exceeded $n_{3He}/n_e \sim 2$ %, direct electron heating by mode converted waves was observed. For the plasmas considered (B_t = 3.6 T, I_p = 2 MA, 37 MHz ICRF, central electron density 3¥10^{19} m^{-3}), the ^{3}He ion cyclotron resonance was central ($R_{ic}(^3He) \sim 2.9$ m); the D ion cyclotron resonance was located far off-axis on the high field side of the plasma ($R_{ic}(D) \sim 2.2$ m) and not easily accessible as it was located on the left of the FW right cut-off ($R_{Rcut-off} \sim 2.4$ m). Here again, the addition of C ions at a concentration $n_C/n_e \sim 2$ % resulted in the presence of the ion-ion hybrid layer associated with the presence of D and C in the plasma at a radius around 2.6 m. Using BIS and FFT analysis of the electron temperature response to ICRF power modulation, direct electron heating around this layer was confirmed experimentally during the ^{3}He minority regime at low ^{3}He concentrations. Numerical simulations performed with the 2-D full wave code CYRANO [19] show that for ^{3}He concentrations of n_{3He}/n_e = 0.5% and without C ions, almost all the power is absorbed by the ^{3}He ions and none is directly absorbed by the electrons. Including C ions at a concentration n_C/n_e = 2 % results in 30% of the power going to the electrons because of the presence of the ion-ion hybrid layer. This parasitic electron absorption is found to decrease as the ^{3}He concentration is increased and the absorption by the ^{3}He ions reaches its maximum for ^{3}He concentrations n_{3He}/n_e of about 1.5 to 2.5 %.

3. MODELLING OF SOL IONIZATION DURING LOWER HYBRID POWER AND GAS PUFFING

In H-mode plasmas in JET, the electron density in the SOL ($n_{e,SOL}$) in front of the lower hybrid (LH) launcher is typically below the cut-off density ($n_{e,cut-off} = 1.7\ 10^{17}\ m^{-3}$ for LH waves at 3.7GHz). In such plasmas, it is possible to obtain good coupling of the LH wave by puffing gas near the launcher using a specially designed gas pipe [20], which leads to a local increase of $n_{e,SOL}$ (i.e. in the flux tube magnetically connected to the gas pipe and the LH launcher). Good LH coupling has also been demonstrated in H-mode plasmas with distances between the last closed flux surface (LCFS) and the LH launcher greater than 10cm [21]. This is important for ITER, where the LH antenna will be situated at least 12cm away from the LCFS. At that location, $n_{e,SOL}$ is expected to be below $n_{e,cut-off}$, based on extrapolations of ITER edge simulations [21]. However, in order to extrapolate the near gas puffing solution

on JET to ITER, it is necessary to understand the physical mechanisms responsible for the increase in $n_{e,SOL}$. Several mechanisms could contribute, e.g. a change in transport or loss of LH power in the SOL leading to an increase of the SOL electron temperature and thus to enhanced ionization of the neutrals in the SOL. To study a possible effect of LH power losses, the fluid code EDGE-2D has been modified to include the effect of the LH wave on the ionisation of the neutral gas in the SOL. In addition, its calculation grid has been enlarged to model shots with a large distance between the LCFS and the LH launcher [22]. Numerical modelling shows that the observed SOL density increase cannot be reproduced with gas puffing alone. However, a very good quantitative agreement can be obtained by assuming an increase of $T_{e,sol}$ due to parasitic LH power losses in the SOL [22]. This is

illustrated in Figs. 4(a) and 4(b), for different combinations of gas puff and SOL heating. As EDGE-2D is a 2D code, the heating values mentioned are for the whole SOL, taken as one large flux tube; an estimate for the power in the flux tube limited to the height of the LH grill can be found by taking into account the ratio of the surface of that limited flux tube to the surface of the LCFS, which is about 20, resulting in 15kW LH power or about 0.5% of the total LH heating for the case considered. The modelled density growth due to SOL heating and gas puff is consistent with the modelled SOL ionization source profiles, Fig.4(b), which for the case with gas puffing and heating are strongly enhanced and extend into the far SOL, contrary to the case without heating and/or without the gas puff. However, this density growth in the SOL is not directly proportional to the SOL ionization source profiles, because e.g. of the influence of parallel transport, which in turn also depends on the temperature profile. This could explain the observed improvement of the LH wave coupling obtained with near grill gas puffing [21].

The modeled density profile for a gas puff of 10^{22} el/s and for 300kW LH power dissipated in the (full) SOL reproduces well the SOL density profiles measured by the reciprocating probe in long plasma limiter distance JET Pulse No's: 58667 and 59817, see Fig.5 [22, 23]. Note that at present EDGE-2D can only model the SOL density up to the limiter (see vertical line in Fig.5); a further extension of EDGE-2D is planned to be able to model the density up to the radius of the launcher.

Further experiments are planned where the gas puff and LH power will be varied. These modeling efforts will be complemented by turbulence measurements, in order to try to estimate the relative importance of enhanced radial plasma transport [24] and enhanced ionization due to LH.

4. STATIONARY COUPLING OF LH POWER AT LARGE DISTANCES BETWEEN PLASMA AND LAUNCHER

One of the main requirements for any heating system for ITER is that it has to provide maximal coupled power regardless of the plasma conditions. A solution for LH coupling in JET has been developed with a specially designed gas pipe, which provides a gas flow near the LH launcher to increase the electron density in front of it. In previous experiments, CD_4 and later D_2 were used, allowing to couple several MW of LH power to the plasma, including distances between the Last Closed Flux Surface (LCFS) and LH launcher up to 10 cm, in plasmas with low triangularity (δ) [20, 21]. However, in order to provide the necessary flexibility for ITER plasma operation good coupling needs to be realized at distances between the LH launcher and the LCFS larger than 10cm. Recent Task Force H experiments in JET have now shown that it is possible to obtain good coupling with distances between the LCFS and the plasma of 15cm, using even less D_2 gas than in earlier experiments. This has been done with a newly developed plasma configuration at for advanced scenario operations (high δ, i.e.$\delta_{lower} = 0.49$ and $\delta_{upper} = 0.4$), which takes advantage of the recent modifications to the divertor in JET. More than 3MW of LH power could be coupled for over 4.5s in a stationary way. This illustrated in Fig.6, showing as a function of time: NBI, ICRH and LH

power delivered, gas puffing rate from the gas pipe (GIM6), reflection coefficient, position of the LCFS (red) and LH launcher (blue) relative to the poloidal limiter (a negative distance means that that launcher is behind the limiter), and the D_α signal showing the ELM activity. Modelling is underway to understand the physics details and for extrapolation to ITER.

SUMMARY

Further detailed analysis of recent experiments has provided new insights in the underlying physical mechanisms at play. The experiments show that ICCD is an effective method to avoid large sawtooth crashes, by keeping the sawtooth period short in discharges with a fast particle population. The main effect in destabilizing the sawtooth consists in changing the shear around the q=1 surface above the critical level. The analysis therefore shows that any method capable of driving a (counter) current close to the q=1 surface would in principle be able to produce the same effect. In depth study of the inverted ICRF heating scenarios shows the importance of the presence of small concentrations of C ions in the discharge on the effectiveness of those heating scenarios. In particular, for the D minority heating scenarios, the C ions act as a sixfold D concentration, and are therefore very effective in moving the ion-ion hybrid layer to the low field side (i.e. much closer to the antenna), therefore making it impossible for the fast wave to reach the ion cyclotron resonance. The effect of C impurities ions is also seen in the ^{3}He minority scenarios but with minor effects in contrast to the scenario with D minority in H, and therefore is the only viable scenario for the non-activated phase of ITER. Modelling of the SOL with strong gas puffing during LH heating shows that agreement with measurements of the ion density profile in the SOL cannot be obtained assuming gas puffing alone. Small parasitic losses of LH power, leading to increased temperatures in the SOL, and thus to enhanced ionization, must be included in the modelling. Recent experiments with LH heating in JET have for the first time demonstrated that stationary coupling of high levels of LH power (3MW) at large distances between plasma and launcher (up to 14 cm) is possible.

ACKNOWLEDGEMENTS

One of the authors (V. Petrzilka) was supported in part by the Czech Grant project GACR 202/04/0360.

REFERENCES

[1]. O. Sauter et al., Phys. Rev. Lett. **88**, 105001 (2002).
[2]. E. Westerhof et al., Nuclear Fusion **42**, 1324 (2002).
[3]. D.F.H. Start et al., in 1992 International Conference on Plasma Physics (Proc. Conf. Innsbruck 1992), Vol. 16C, Part II, European Physical Society, Geneva (1992) p. 897.
[4]. V.P. Bhatnagar, et al., Nuclear Fusion **34**, 1579 (1994).
[5]. M.J. Mantsinen, et al., Plasma Physics and Controlled Fusion **44**, 2521 (2002).
[6]. M.-L. Mayoral, et al., Physics of Plasmas **11**, 2607 (2004).

[7]. F. Porcelli, D. Boucher and M.N. Rosenbluth, Plasma Physics and Controlled Fusion **38**, 2163 (1996).
[8]. L.-G. Eriksson et al., Physical Review Letters **92**, 235004 (2004).
[9]. L.-G. Eriksson et al., Nuclear Fusion **46**, S951 (2006).
[10]. J. Hedin, T. Hellsten, J. Carlsson, Proc. of Joint Varenna-Lausanne Workshop on "Theory of fusion Plasmas" 467, Varenna (1998).
[11]. J. Hedin et al., Nuclear Fusion **42**, 527 (2002).
[12]. J. Graves et al. Proc. of Joint Varenna-Lausanne Workshop on "Theory of fusion Plasmas", Varenna (2006), to appear.
[13]. M.-L. Mayoral et al., Nuclear Fusion **46** (2006) S550-S563.
[14]. D. Van Eester, Plasma Phys. and Control. Fusion **42** (2004) 1675-1697.
[15]. E.A. Lerche and D.Van Eester, submitted to Plasma Phys. and Control. Fusion in 2005
[16]. D. Van Eester and R.Koch, Plasma Phys. and Control. Fusion **40** (11) (1998) 1949-1976.
[17]. I. Monakhov et al., Physics of Plasmas **6** (3) (1999) 885-896.
[18]. J.C. Wrigth et al, Physics of Plasmas **11(5)** (2004) 2473-2479
[19]. P.U. Lamalle, LPP-ERM/KMS Lab. Report **101**, Brussels (1994)
[20]. V. Pericoli-Ridolfini, et al., Plasma Phys. Contr. Fusion **46** (2004) 349-368.
[21]. A. Ekedahl, et al., Nucl. Fusion **45** (2005) 351-359.
[22]. V. Petrzilka, et al., EPS Rome 2006 Conference, paper P-1.067; Nuclear Fusion, to be published.
[23]. G. Granucci et al., 30th EPS Conference, St. Petersburg, ECA **27A** (2003), P-1.191.
[24]. G.F. Matthews, et al., Plasma Phys. Contr. Fusion **44** (2002) 689.

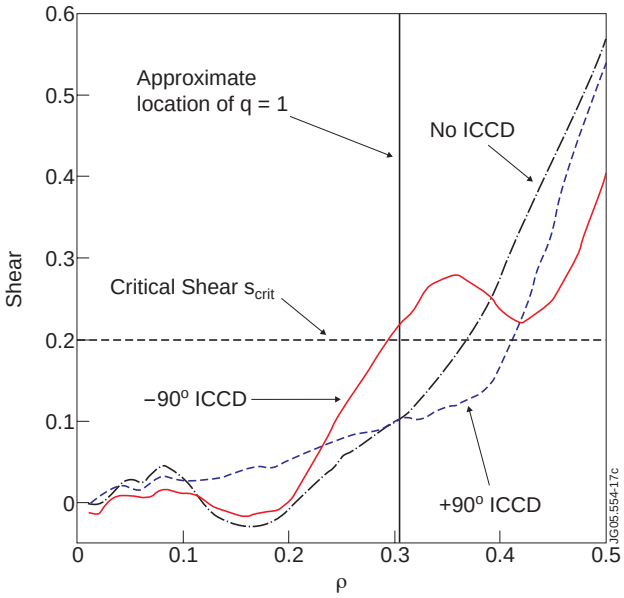

Figure 1: Simulated magnetic shear profile for JET Pulse No: 58934 during the sawtooth destabilisation phase with off-axis co-current propagating ICCD (-90^o phasing), solid line; the same target parameters but with off-axis counter propagating ICCD ($+90^o$ phasing), dashed line; the same target parameters but without ICCD (only central heating), dot-dashed line.

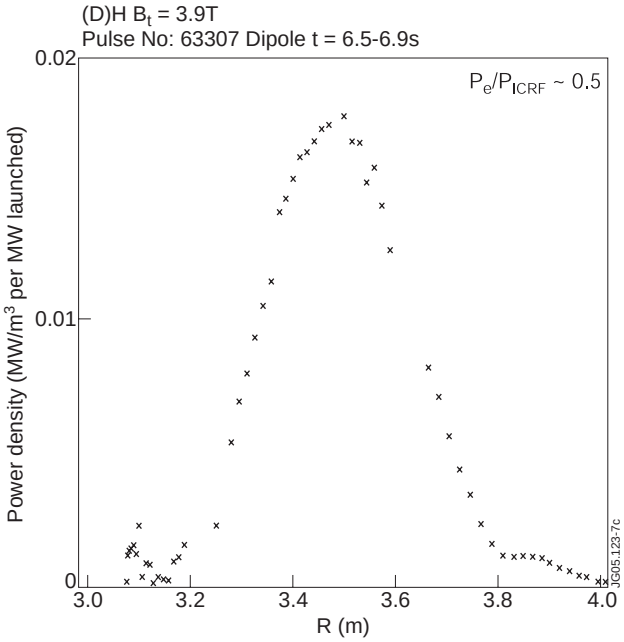

Figure 2: Typical deposition profile for direct electron heating with D minority heating in a H plasma (from Break-In-Slope (BIS) analysis).

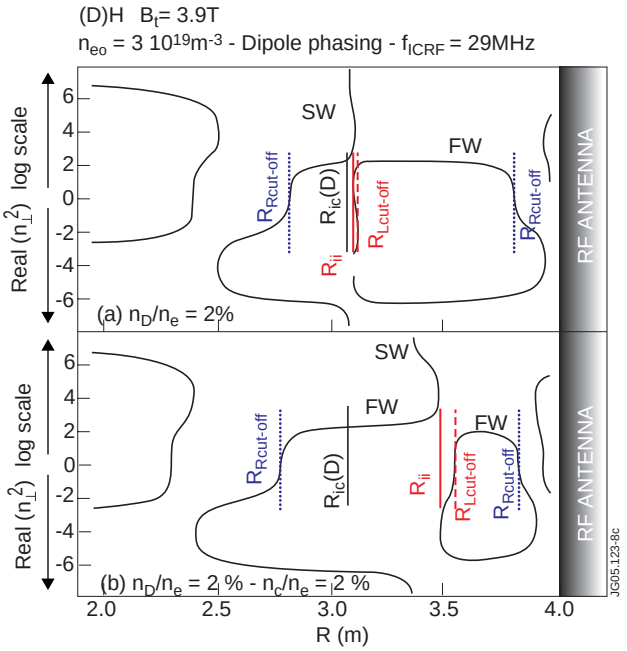

Figure 3: Real part of the square of the perpendicular refractive index $n_\perp$ from the resolution of the cold plasma dispersion relation. Fast wave (FW) and slow wave (SW) branches are represented as well as the FW left cut-off $R_{Lcut\text{-}off}$; FW right cut-off $R_{Rcut\text{-}off}$; FW resonance R_{ii} and D cyclotron resonance R_{ic}. Two cases are plotted: (a, top) with n_D/n_e = 2 % in a H plasma and (b, bottom) with n_C/n_e = 2 % and n_D/n_e = 2 % in a H plasma.

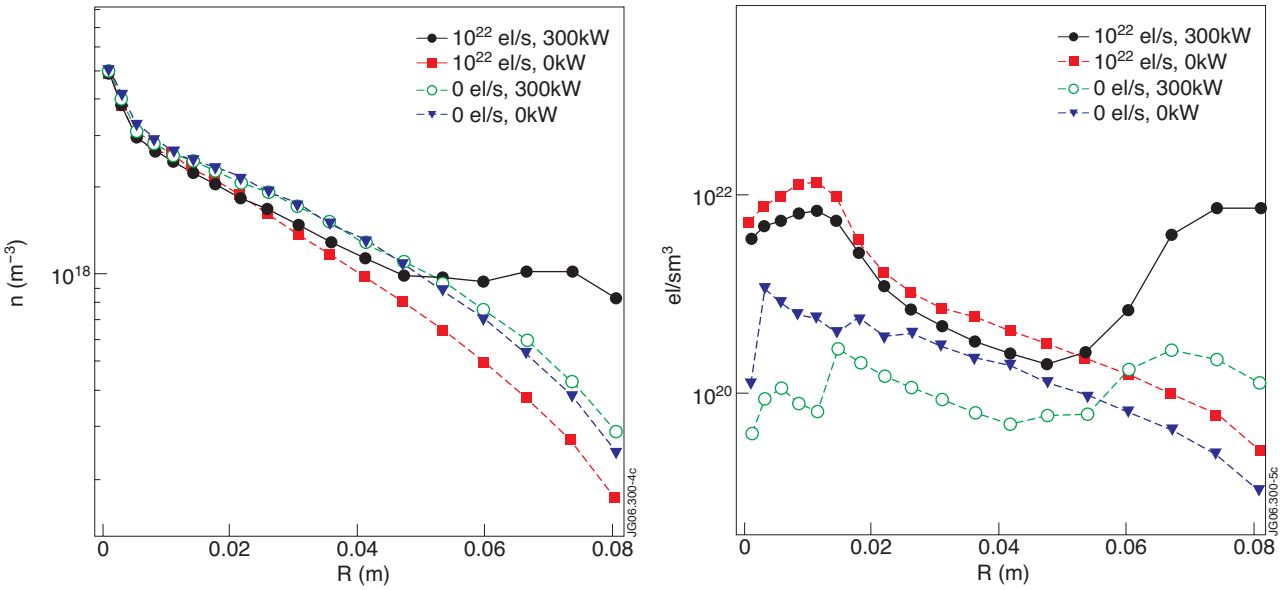

Figure 4(a): (left) and (b) (right): SOL density (left) and ionization source (right) profiles for various near grill gas puffing and SOL LH heating rates, r is the distance from the separatrix (at 0 cm) to the limiter (at 8 cm).

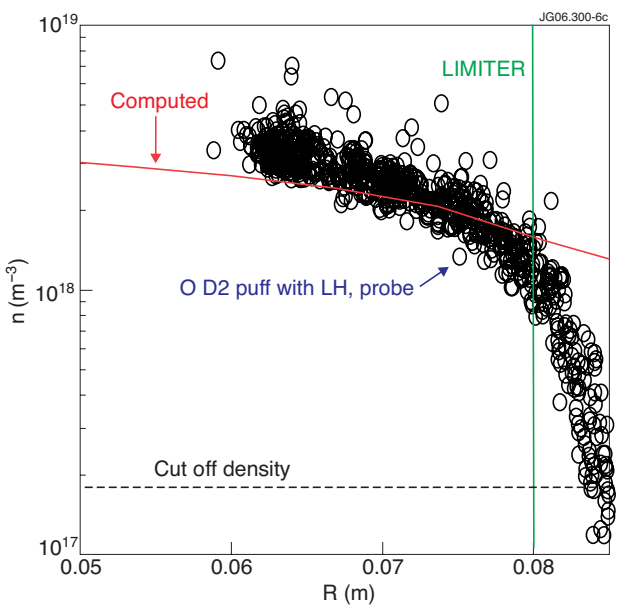

Figure 5: Comparison of modelled density profile (red line) with data (blue dots). Modelling is only valid up to the limiter (green vertical line).

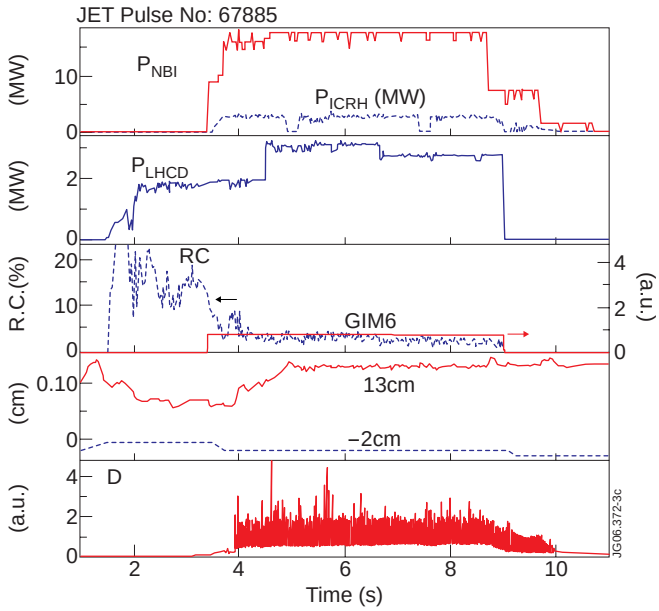

Figure 6: Illustration of long pulse high power LH coupling at large plasma-launcher distances Shown are as a function of time: NBI, ICRH and LH power delivered, gas puffing rate from the gas pipe (GIM6), Reflection Coefficient (RC), position of the LCFS (red) and LH launcher (blue) relative to the poloidal limiter (a negative distance means that that launcher is behind the limiter), and the D_α signal showing the ELM activity.